

Article

# Influences of Restaurant Waste Fats and Oils (RWFO) from Grease Trap as Binder on Rheological and Solvent Extraction Behavior in SS316L Metal Injection Molding

Mohd Halim Irwan Ibrahim <sup>\*</sup>, Azriszul Mohd Amin <sup>†</sup>, Rosli Asmawi <sup>†</sup> and Najwa Mustafa

Advanced Manufacturing and Materials Center, University Tun Hussein Onn Malaysia (UTHM), Parit Raja, Batu Pahat, Johor 86400, Malaysia; azriszul@uthm.edu.my (A.M.A.); roslias@uthm.edu.my (R.A.); nj.wawa@gmail.com (N.M.)

<sup>\*</sup> Correspondence: mdhalim@uthm.edu.my; Tel.: +6-07-453-7981; Fax: +6-07-453-6080

<sup>†</sup> These authors contributed equally to this work.

Academic Editor: Hugo F. Lopez

Received: 4 November 2015; Accepted: 18 December 2015; Published: 2 February 2016

**Abstract:** This article deals with rheological and solvent extraction behavior of stainless steel 316L feedstocks using Restaurant Waste Fats and Oils (RWFO) from grease traps as binder components along with Polypropylene (PP) copolymer as a backbone binder. Optimal binder formulation and effect of solvent extraction variables on green compacts are being analyzed. Four binder formulations based on volumetric ratio/weight fraction between PP and RWFO being mixed with 60% volumetric powder loading of SS316L powder each as feedstock. The rheological analysis are based on viscosity, shear rate, temperature, activation energy, flow behavior index, and moldability index. The optimal feedstock formulation will be injected to form green compact to undergo the solvent extraction process. Solvent extraction variables are based on solvent temperature which are 40 °C, 50 °C, and 60 °C with different organic solvents of *n*-hexane and *n*-heptane. Analysis of the weight loss percentage and diffusion coefficient is done on the green compact during the solvent extraction process. Differential Scanning Calorimeter (DSC) is used to confirm the extraction of the RWFO in green compacts. It is found that all binder fractions exhibit pseudoplastic behavior or shear thinning where the viscosity decreases with increasing shear rate. After considering the factors that affect the rheological characteristic of the binder formulation, feedstock with binder formulation of 20/20 volumetric ratio between PP and RWFO rise as the optimal binder. It is found that the *n*-hexane solvent requires less time for extracting the RWFO at the temperature of 60 °C as proved by its diffusion coefficient.

**Keywords:** restaurant waste fats and oils (RWFO); binder formulation; rheological behavior; solvent debinding variables

## 1. Introduction

Metal injection molding (MIM) is a manufacturing process with an advantage of producing intricate and small parts in high volume production with a few shot as compare to other fabrication processes [1–4]. The process involves in developing the feedstock from metal powder and multi components of binder which are then injected by injection molding process to form desired shapes. The components then undergo a debinding process to remove the binder and, finally, a sintering process.

316L stainless steel is one of the most widely used materials for industrial applications. Since 316L stainless steel is a highly alloyed material with good mechanical and corrosion properties it is widely recognized as material for implants [5].

Binder in feedstock is crucial since it will influence the formability of the metal powder into the desired shape [6]. Usually binders are constituted of polymer as backbone binder and other additives for improving flow, wettability, and reducing agglomeration of powder particles. Due to these reasons, good rheological behavior is important since it influences the shape retention of the green compacts during injection molding process [7]. Binders ranging from commercial polymer/wax to sustainable binder from food grade materials have long been successfully implemented as binders in MIM. Although variety of binders have been applied in the MIM process, a sustainable binder is preferable as stated in Brandtland report [8]. Many sustainable binders from food grade materials have been explored in MIM such as carnauba wax [9–11], bees wax [12], palm stearin [13], and palm kernel [14,15]. Although these sources of binders have several advantages, they have some conflict issues between being a human source of foods and industrial sector needs which in turn could rise its price and will disrupt the foods chain of the human population [16].

Debinding is a crucial process of removing binder from green compacts since improper selection of debinding variables could lead to component defects such as cracks and swells [17]. Various techniques can be implemented for the debinding process ranging from thermal, wicking, and solvent. With the shortest time and least impact on the part, the solvent extraction process is preferable since it could result in time and cost savings for both solvent and thermal debinding processes [18]. Solvent is used to remove low molecular weight binder components, which results in porosity inside the components. The existence of porosity inside the components is connected to forming channels that minimize part distortion due to pressure built up inside the components and allow the degradation of the backbone binder to diffuse on the surface easily during a thermal debinding process [19]. Many factors can influence the time taken from solvent extraction process such as the thickness of a part, solvent temperature, types of solvents, and the solvent's flow rate.

Restaurant waste fat and oil (RWFO) derivatives from grease traps have long been analyzed as a potential feedstock for biodiesel [16,20] due to its numerous amounts of fatty acids (Oleic, Stearic, Palmitic and *etc.* [21,22]) which come from animal waste fat and cooking oil [23,24]. Furthermore, its properties of non-toxicity, biodegradability, and renewability [16] make it more interesting for use in biodiesel, cosmetics products, and even as a soap products. With rapids growth of human population, urbanisation, lifestyle changes and nutrition transition has made the RWFO become a more interesting topic in sustainable development [25–27]. Although it is well known for its properties of various fatty acids, its implementation in MIM has not being explored extensively yet [28] and therefore RWFO derivatives as binder components for SS316L feedstock are tested and analyzed in terms of rheological behavior and solvent extraction process.

## 2. Experimental Section

Water atomized 316L stainless steel powder with chemical composition and particle size distribution as shown in Tables 1 and 2 respectively has irregular shape as revealed in Figure 1b. Particle size distribution is obtained using laser scattering particle analyser FRITSCHE Analysette 22 (Universiti Tun Hussein Onn Malaysia (UTHM), Johor, Malaysia) since it is one of the important factors in MIM which influenced the different stages of the MIM process [29]. The selected stainless steel powder is found to have 64.8% Critical Powder Volume Concentration (CPVC) (Figure 1a). CPVC is the point where all the particles are tightly packed and all voids between the particles are filled with binder. The determination of CPVC is important in order to establish the optimum amount of binder in the feedstock. CPVC was experimentally determined by means of oil absorption ASTM D-281-31 method using Thermo Haake Rheomix mixer (Universiti Kebangsaan Malaysia (UKM), Selangor, Malaysia) where 0.5 mL volume of oleic acid was added to 200 g of SS316L powder for every 5 min [30]. If the addition of oil continues, the torque value decreases abruptly indicating that the critical powder volume concentration is reached [31]. Equation (1) is employed to obtain the CPVC using powder volume ( $V_p$ ) and acid oleic volume ( $V_o$ ) at the point where the torque is a maximum.

$$\text{CPVC} = \frac{V_p}{V_p - V_o} \times 100\% \quad (1)$$

For MIM feedstock, 2% to 5% volumetric powder loading below the CPVC value is suitable [1]. Volumetric powder loading plays a significant role in preventing parts from slumping or distorting which, in this case 60%, volumetric powder loading (approximately 5% below the CPVC value) was used as SS316L feedstock.

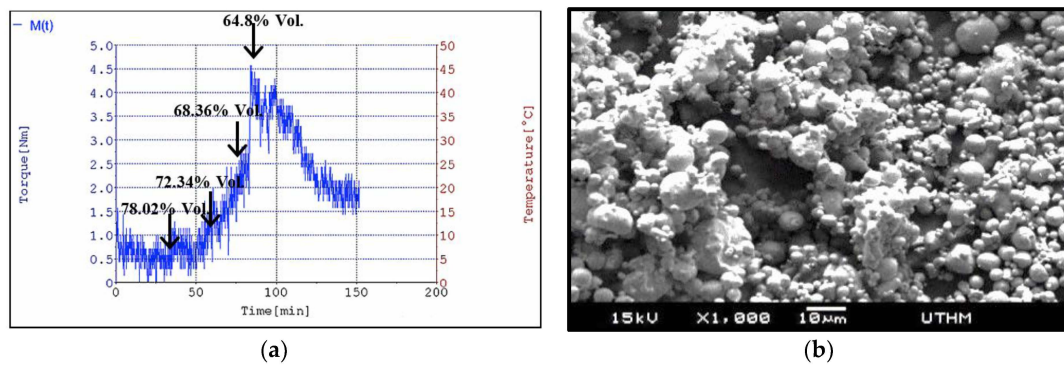


Figure 1. (a) CPVC of water atomized SS316L powder [30]; (b) Powder morphology.

Binder consisting of Polypropylene (PP) supplied by Lotte Chemical Titan (Johor, Malaysia) Sdn Bhd is used as a backbone binder and RWFO from a grease trap supplied by Perniagaan Seri Gunung (Selangor, Malaysia) Enterprises is used as primary binder for lubrication and wettability. Thermal characteristics of binder components are shown in Table 3 by using Differential Scanning Calorimeter (DSC, UTHM, Johor, Malaysia) and Thermalgravimetric Analysis (TGA, UTHM, Johor, Malaysia) for melting and degradation temperature, respectively.

Table 1. Chemical composition of water atomized SS316L powders supplied by Epson Atmic Corp., Aomori Prefecture, Japan (wt. %).

Composition wt. %									
Fe	C	Si	Mn	P	S	Ni	Cr	Mo	Cu
Balance	0.027	0.84	0.19	0.016	0.012	12.2	16.4	2.1	0.03

Table 2. Characteristic of SS316L powders supplied by Epson Atmic Corp. Japan.

$D_{10}$ ( $\mu\text{m}$ )	$D_{50}$ ( $\mu\text{m}$ )	$D_{90}$ ( $\mu\text{m}$ )	Pycnometric Density ( $\text{g}/\text{cm}^3$ )	Tap Density ( $\text{g}/\text{cm}^3$ )
2.72	6.70	15.74	8.0471	4.06

Fourier Transform Infrared (FTIR, UTHM, Johor, Malaysia) was used as a tool to quantify the RWFO received and analysis was done on five samples with different lot of RWFO with the same provider for characterizing the chemical bonds corresponding to various functional groups (Figure 2) [32,33].

Powder and binder volumetric or weight percentage employed in this work are shown in Table 4. Differential Scanning Calorimeter (DSC) analysis was conducted to determine the melting temperature of the binder components and these experiments were performed using DSC TA Instruments Q20 where the samples were heated from room temperature up to 200 °C at 5 °C/min (Figure 3) and then cooled at the same rate under 50 mL/min Nitrogen atmosphere. Thermalgravimetric analysis (TGA) were performed on a LINSEIS Thermobalance from room temperature up to 600 °C at a heating rate

of 10 °C/min (Figure 4) in air atmosphere in order to determine decomposition temperature of the binder components.

Powder binder mixtures were carried out in a Brabender Plastograph EC (UTHM, Johor, Malaysia) at 175 °C temperature, rotor speed of 30 r.p.m and for 90 min duration. Mixing temperature was selected based on DSC and TGA experiments that was below the lowest degradation temperature of the binder components and had to be higher than the highest melting temperature of the binder components. The feedstock paste was then crushed into small pellets using a granule machine for easy feeding into the capillary rheometer and injection machine. TGA was performed on every feedstock formulation for monitoring the existence of the binder components.

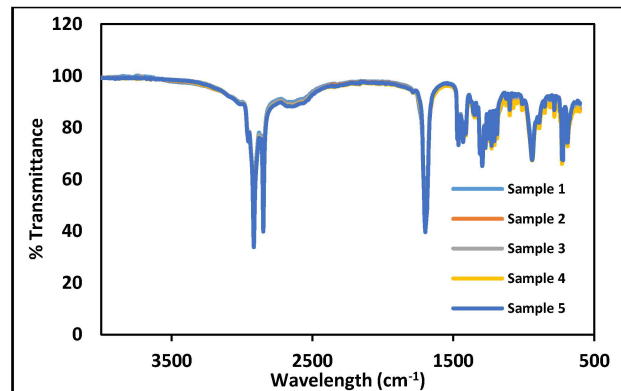


Figure 2. FTIR profile of 5 samples RWFO.

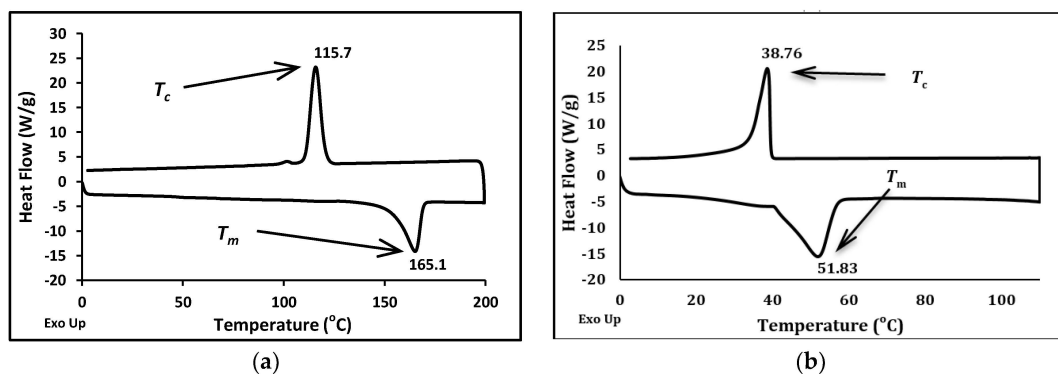


Figure 3. DSC analysis of (a) polypropylene (b) RWFO in nitrogen atmosphere with heating and cooling rate of 5 °C/min to determine the melting and crystalline temperature ( $T_m$  and  $T_c$  respectively).

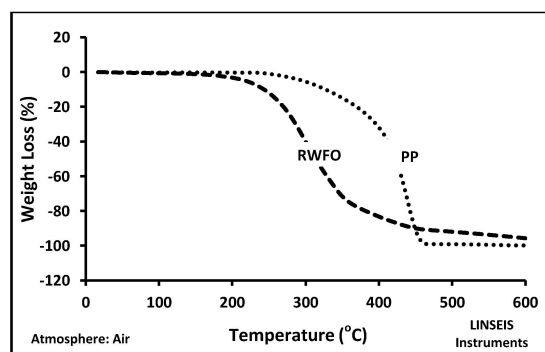


Figure 4. TGA analysis of Polypropylene and RWFO in air atmosphere and heating rate of 10 °C/min to determine degradation temperature of binder constituents.

Rheological behavior of the feedstocks was determined by Instron CEAST SmartRHEO 10 (Universiti Teknikal Malaysia (UTeM), Melaka, Malaysia) with die dimensions of 1 mm in diameter and length 20 mm in order to keep a  $L/D$  ratio of 20. The shear rate was chosen in the range of 1000 to 10,000  $s^{-1}$  and a preheat time of 5 min was employed. The effect of temperature on rheological behavior of all feedstock formulations was done with the temperatures of 170 °C, 180 °C, and 190 °C, respectively.

Selected feedstock formulation based on rheological analysis was undergone in the injection process using NISSEI NP 7 Real Mini injection machine (UTHM, Johor, Malaysia). The injection molding parameters were optimized using Taguchi methods (will not be discussed in this paper) as shown in Table 5.

**Table 3.** Characteristic of binder and pure components ( $T_m$  and  $T_d$  are melting temperature and decomposition temperature respectively).

Material	Density (g/cm <sup>3</sup> )	$T_m$ (°C)	$T_d$ (°C)
PP	0.9	165	440.5
RWFO	0.9	52	297.7

**Table 4.** Components and contents used for 60% volumetric powder loading (93 wt. %) of feedstocks.

Formulation	SS316L Powder (vol. %/wt. %)	Binder Composition and Contents (vol. %/wt. %)
F1	60/93	PP (24/4.2) + RWFO (16/2.8)
F2	60/93	PP (20/3.5) + RWFO (20/3.5)
F3	60/93	PP (16/2.8) + RWFO (24/4.2)
F4	60/93	PP (12/2.1) + RWFO (28/4.9)

**Table 5.** Injection molding parameter for F2 feedstock.

Injection Temperature (°C)	Injection Pressure (MPa)	Mold Temperature (°C)	Cool Time (s)	Injection Speed (RPM)	Injection Time (s)	Packing Time (s)
165	80.4	40	15	105	1	2

### 3. Results and Discussion

#### 3.1. FTIR and Thermal Analysis of Binder

FTIR analysis is important since RWFO, which comes from different restaurant location of grease traps are collected and mixed in storage, might influence inconsistency rheological behavior of the feedstock produced. As shown in Figure 2, the results of the FTIR indicates no significant changes in the properties of the RWFO, which confirm the consistency of the constituents in the RWFO.

The melting temperature ( $T_m$ ) along with crystalline temperature ( $T_c$ ) can be observed at approximately  $T_m = 52$  °C,  $T_c = 38.8$  °C for RWFO and  $T_m = 165$  °C,  $T_c = 115.7$  °C for PP, respectively (Figure 3). Results of TGA curves show the degradation temperature of binder components occurs at the interval of 200 °C to 600 °C and 250 °C to 450 °C, respectively (Figure 4). From these results, mixing temperature of the powder and binder components was selected below than the lowest degradation temperature and higher than the highest melting temperature of the binder components. Data of the degradation and melting temperature of the binder components also will be used as guideline for solvent and thermal debinding process. Information regarding crystalline temperature (Figure 3) of the RWFO and PP is used as the guidelines for mold temperature since crystalline temperature is a transition temperature for substances to form a solid from a liquid state.

The DSC scans obtained for the feedstocks with different binder formulation is presented in Figure 5a. All the peaks are endothermic which show the melting point depression of the PP and RWFO in the different feedstock formulation, respectively. Figure 5a includes the binder components'

scans at the top and the feedstock formulation DSC scans at the bottom. It is apparent that the melting peaks of the blends displaced to the left with respect to the peaks of the binder components. For instance, the melting point depression of PP is larger with respect to RWFO for F4 feedstock formulation. The melting point depression was attributed to changes in crystal size because of the presence of the other components in the blends. This reason seems reasonable when considering the way the melting points were obtained [34]. During DSC analysis, the RWFO were first melted followed by PP in succession until the blend was in the liquid state and then quenched, freezing up the melt structure. During the quenching phase, the blend crystallized in a sequence that depended on the rate of crystallization of the polymers. In this regard, the PP crystallized first, then finally the RWFO. In this process, RWFO not yet crystallized could have been “enclosed” in the crystalline structure of a PP already crystallizing reducing the space available for crystallites. This phenomena would explain the reduction of crystallite size and hence, in melting point of RWFO and PP [34].

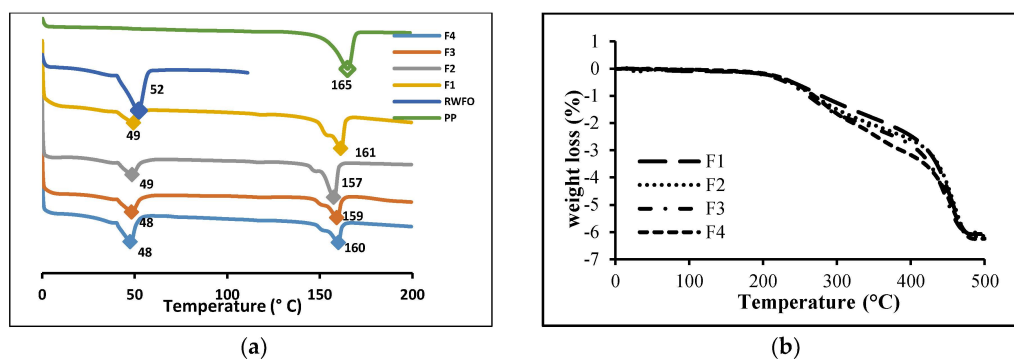


**Figure 5.** (a) DSC scans of the PP, RWFO and feedstock formulation; (b) TGA profile of different feedstock formulation.

The resulting TGA curves for different binder formulation at a heating rate of 10 °C/min are presented in Figure 5b. The theoretical values of the maximum percentage weight loss possible for these systems are approximately 7%. At the temperature of 500 °C the binder was presumably burned off completely. For F1 feedstock the estimated percentage weight loss of the RWFO is 2.5% and the remaining weight loss is due to the degradation of PP. The evaluation continues with F2 where the estimated of RWFO degradation is 2.9%, followed by F3 which is 3.0%, and finally F4 3.7%. The deviation of TGA profiles between the binder formulations is due to the different weight contents of RWFO and PP in each of the feedstock formulation. The deviation of the total degradation of binder components with respect to the calculated one is due to some binder being left inside the mixer, which reduces its quantity. This also indicates that the miscibility of the binder components with the SS316L powder was good which is crucial in avoiding powder agglomeration [34]. The TGA analysis also suggests that degradation of binder components has not occurred during mixing process. Two degradation slopes were observed which related to RWFO and PP that indicates both components were intact with SS316L powder.

### 3.2. Rheological Behavior

The rheological behavior of feedstock is crucial to evaluate the ability of mixtures to be injected. The capillary test is the best approach to predict the flow behavior during injection molding. Four different feedstock formulations are shown in Figure 6. It can be observed that the viscosity of all the feedstock decreases with increasing shear rate which indicates pseudoplastic behavior [1] and leads to good wettability of the binder and metal powder [35]. The shear rate range of 100 s<sup>-1</sup> to 10,000 s<sup>-1</sup> was selected because it is similar shear rate values obtained during injection stage [31]. For the feedstock to be successfully injected, viscosity values recommended for MIM process must be less than 100 Pa.s for viscosity and 100 s<sup>-1</sup> to 10,000 s<sup>-1</sup> in shear rate [31,36].

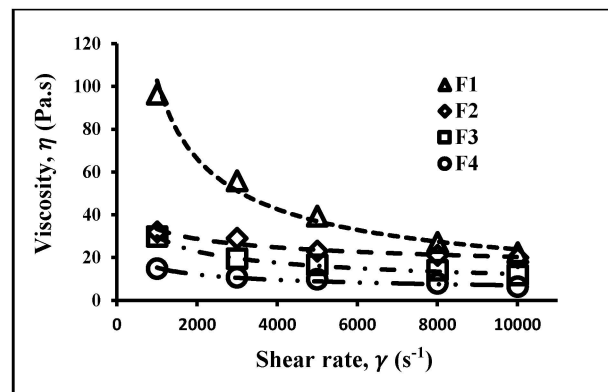


**Figure 6.** Effect of shear rate on viscosity changes at 170 °C for different binder formulation.

From Figure 6, flow behavior index,  $n$  was calculated from the Equation (2).

$$\eta = K\gamma^{n-1} \quad (2)$$

where  $\eta$  is the viscosity,  $\gamma$  is the shear rate, and  $K$  is a constant. The value of  $n$  indicates the degree of sensitivity of viscosity against shear rate. In the case of MIM process, feedstock must have pseudoplastic behavior where  $n < 1$ . Higher the ratio of RWFO will aid the viscosity of the blends. When more RWFO being used in the blends, the lower the viscosity of the feedstock. This is due to the RWFO has the lubricating effects which lowering the friction between molecules polymer and hence lower stresses needed in deforming the fluid [37]. From Figure 6, feedstock with binder formulation of F4 has the lowest viscosity against the shear rate compared to other feedstock formulations.

The sensitivity of viscosity versus shear rate is higher for F1 binder as compared to other binder formulations. This indicates that the F1 formulation highly depends on shear rate and temperature in aiding the flow of the binder due to greater amounts of PP, which is viscous to flow. Other formulations show lower sensitivity due to the amounts of RWFO being higher which indicates that only a small value of shear rate is needed to aid the flow of the feedstock because most of the flow behavior was contributed to by lubrication from RWFO.

Although the  $n$  value shows all the binder formulation can be injected, analysis of activation energy base on the Arrhenius equation (Equation (3)) also need to be considered.

$$\ln(\eta_T) - \ln(\eta_0) = E_a/RT \quad (3)$$

From Equation (3),  $E_a$  is the flow activation energy,  $R$  is the gas constant,  $T$  is the temperature,  $\eta_0$  is the viscosity at reference temperature. If the value of  $E_a$  is lower, the viscosity is not so sensitive to temperature variation, which means that any small fluctuation of temperature would not give any sudden viscosity change [37]. The value of  $E_a/R$  can be calculated from the gradient of the graph shown in Figure 7. The graph presented in Figures 8 and 9 show the evolution of  $n$ ,  $\eta_0$  and  $E_a$  rheology parameters with variations of feedstock formulation for the reference conditions of 170 °C and 1000 s<sup>-1</sup>. A shaded region is the sudden variation of all rheological parameters ( $n$ ,  $\eta_0$  and  $E_a$ ) occurs at F1–F2 feedstock formulation. This region can be considered as critical feedstock formulation based on the 60% volumetric powder loading. A similar region was found by Hidalgo *et al.* [38] with critical powder loading but in this case for feedstock formulation. Minimum activation energy is obtained for the F2, being the feedstock less sensitive to temperature variations. This minimum marches with a maximum of the  $\eta_0$  parameter and an inflection point in the value of the flow index.

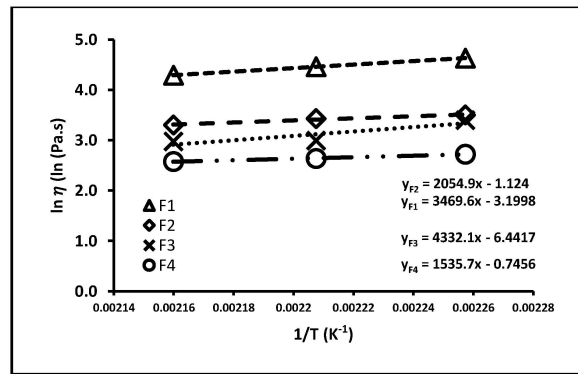


Figure 7. Dependence of shear viscosity with temperature for different feedstock formulations.

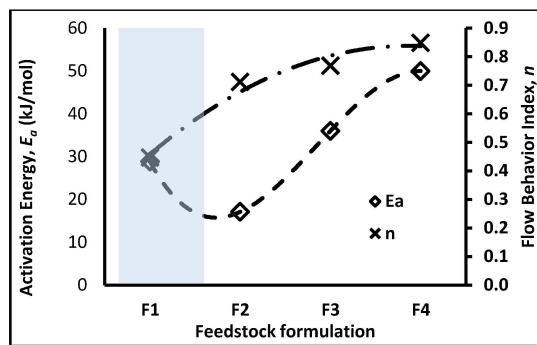


Figure 8. Determination of critical feedstock formulation between  $E_a$  and  $n$ .

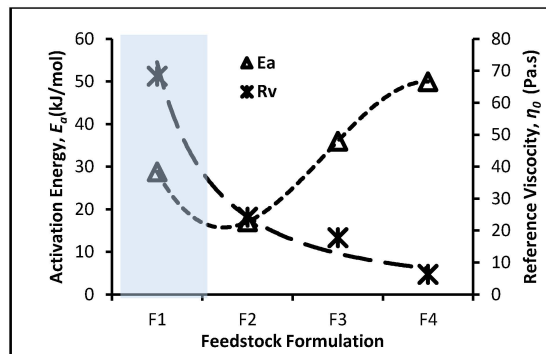


Figure 9. Determination of critical feedstock formulation between Activation energy,  $E_a$  and Reference viscosity,  $\eta_0$ .

In the above paragraphs, rheology parameters were independently studied and plotted in dissimilar axes giving unclear or inadequate insights for optimal feedstock formulation. A general moldability index  $\alpha_{stv}$  is proposed to summarize and globally describe the rheological behavior of a feedstock taking into account all the parameters [37,38]. The subscripts s, t, and v represent the shear sensitivity, temperature sensitivity, and viscosity, respectively. The general moldability index is defined as in the Equation (4);

$$\alpha_{stv} = \frac{1}{\eta_0} \frac{\left| \frac{\partial \log \eta}{\partial \log \gamma} \right|}{\left| \frac{\partial \log \eta}{\partial \left( \frac{1}{T} \right)} \right|} = \frac{1}{\eta_0} \frac{1-n}{E/R} \tag{4}$$

where  $\eta_0$  is the reference viscosity at 170 °C and shear rate of 1000 s<sup>-1</sup>. Higher value of  $\alpha_{stv}$  indicates better feedstock formulation. From Figure 10, F2 shows the better general moldability index and this feedstocks will be injected and be analyzed for solvent debinding variables.

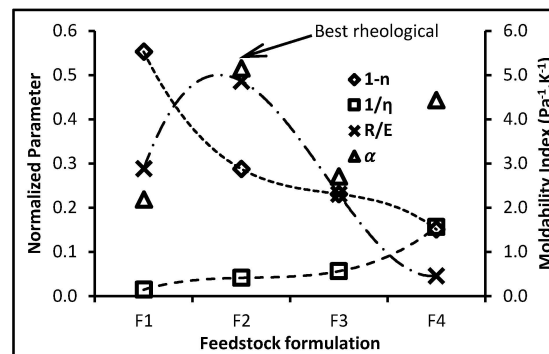


Figure 10. General moldability index vs. feedstock formulation.

### 3.3. Solvents Debinding Behavior

The goal in solvent debinding is to remove the low molecular weight of binder components, which in this case is RWFO, in the shortest time with the least impact on the green molded part. Weight loss of the green compact after solvent extraction was monitored by replication. As can be seen in Figure 11b,c, solubility of the RWFO with hexane solution is good. The colorless hexane solution changes to an orange color, which indicates the existence of extraction process of RWFO.

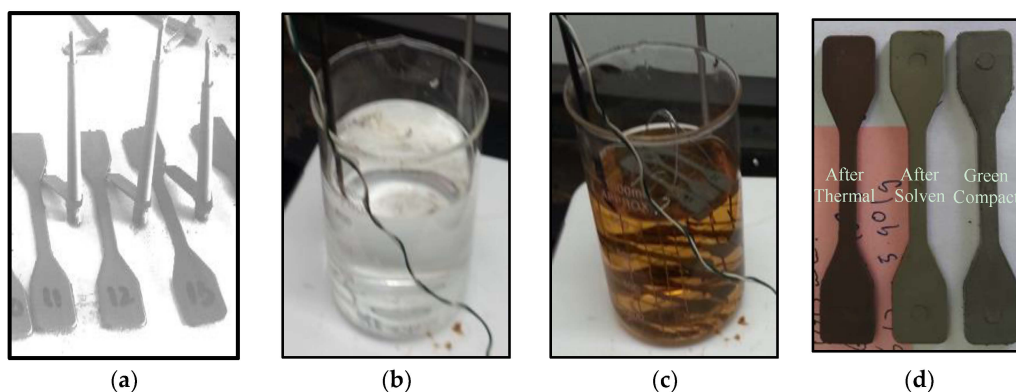


Figure 11. (a) Injected part (b) Colorless Hexane (c) Color of the hexane solvent changing to orange after green compact being immersed into it during the third hour; (d) comparison of part dimension after thermal and solvent extraction with green compact.

Temperature effect is one of the important variables in the solvent extraction process (Figure 11). There was no indication of swelling or cracks found on the components after solvent extraction process at 60 °C temperature with both solvents. Weight loss analyses were done to monitor any changes in weight after being undergone the solvent extraction process. The diffusion coefficient relation was to determine the rate of diffusion of the RWFO from the green compact. Figure 12 shows result of the solvent extraction process during the first hour with different solvent temperatures and organic solvents.

Weight loss percentage of the green part was calculated base on Equation (5) where  $W_i$  is the initial weight of the green part and  $W_a$  is the weight of the green part after solvent debound.

$$W_{\text{loss}} = \frac{W_i - W_a}{W_i} \times 100\% \quad (5)$$

Using Equation (6), the diffusion coefficient was calculated for RWFO extraction in both Hexane and Heptane solvents where  $C_a$  is the average concentration of binder remaining on compressed part,  $C_i$  is the initial concentration of binder,  $C_0$  is the boundary condition (zero),  $t$  is the debinding time,  $D$  is the debinding coefficient and  $h$  is the thickness of the compressed part (Nanjo *et al.*, 1993 cited in [18]).

$$\frac{C_a - C_0}{C_i - C_0} = \frac{8}{\pi} e^{-\frac{\pi^2}{h^2} Dt} \quad (6)$$

Percentage weight loss and diffusion coefficient of green part is increased with temperature from 40 °C to 60 °C using organic solvents of Hexane and Heptane at a fixed solvent to feed ratio (S/F = 14:1) during the first hour. This indicates that RWFO is soluble in both solvents and able to extract RWFO from the green part. During the first hour, Hexane organic solvent shows significant percentage weight loss as compare to Heptane for 40 °C to 60 °C solvent temperature. Diffusion coefficients also increase with temperature that explained the proportional increase in percentage weight loss of the green part. This shows that hexane solvents have better extraction of RWFO as compared to heptane and this might due to the lower carbon number of hexane which increases the solvent diffusion rate into the RWFO [17].

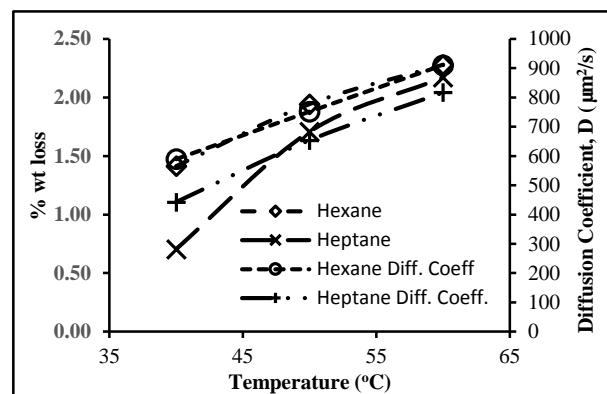


**Figure 12.** Percentage weight loss and diffusion coefficient at different temperatures during first hour of solvent extraction for F2 feedstock formulation.

From Figure 13, using hexane as the choice of organic solvent, the total amount of RWFO extracted increases by increasing the extraction time from 1 to 3 h, whereas increasing the extraction time from 5 to 6 h does not give any significant change of weight loss percentage on the part. Also as the total percentage weight loss was increase, the diffusion coefficient decreased with time. This is true as stated by Fick's 2nd Law that fluid migration in the matrix occurs mainly through diffusion and concentration drive this migration [39]. During the first hour, concentration of the RWFO was higher in the green compact and reducing after several hours during extraction process. The percentage weight loss is stabilized after 3 h, which reaches about 3 wt. % loss of RWFO. This means that the total amount of binder extracted is not affected by increasing the extraction time over 3 h. The diffusion coefficient of RWFO decreases clearly from 868 to 223.6  $\mu\text{m}^2/\text{s}$  by increasing the extraction time from 1 to 10 h.

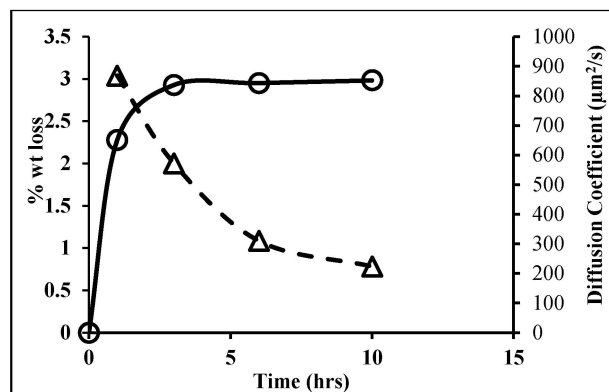


**Figure 13.** Percentage weight loss and diffusion coefficient of green part using Hexane at temperature of 60 °C.

The green compact after solvent debound for 3 h were then undergoing DSC analysis to monitor the remaining RWFO in the green compact. From Figure 14a, initially two peaks are observed indicating two binder components exist in the green compact. After solvent extraction process, RWFO peaks vanish which leaves only PP melting and crystalline temperature peaks (Figure 14b). This analysis was done on the sample taken from the center of the green compact after solvent extraction had taken place. This indicates that the RWFO were successfully extracted out of the green compact. From Scanning Electron Microscope (SEM) image and Energy dispersive spectroscopy (EDS) analysis (Figure 15a), it can be seen that most of the powder particles are covered by PP and RWFO. Figure 15b shows the results of porosity existence inside the green compact leaving only PP to hold the powder particles after 3 h solvent extraction process. The existence of porosity inside the green compact would create a channel that helps the diffusion of degraded PP during thermal debinding process. Carbon content from the green compact also reduced due to the disappearance of RWFO from the green compact as can be seen on the first peaks of each EDS profile. Figure 11d shows the comparison of the dimensional changes of the green compact before and after the solvent extraction process. No significant dimension changes can be seen on the components. After undergoing thermal debinding process, significant changes in dimension are observed where about 1% shrinkage occurs (will not be discussed in this paper).

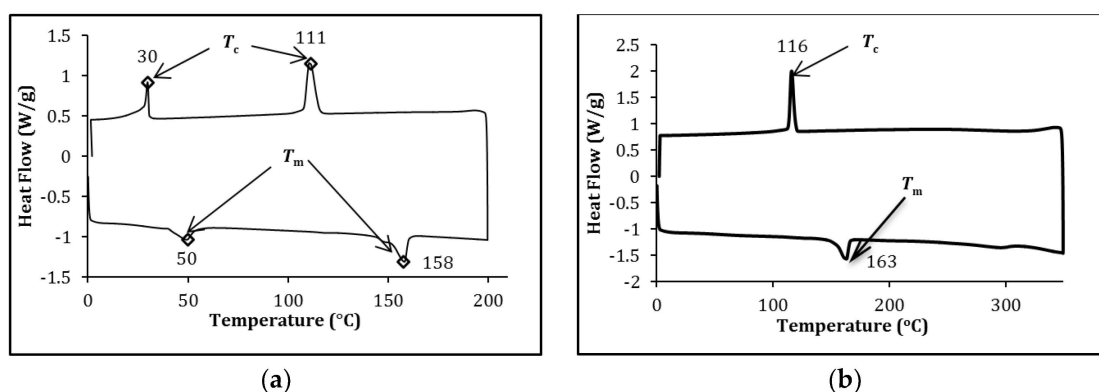


**Figure 14.** DSC scan of the (a) F2 green compact; (b) after solvent extraction under 50 mL/min Nitrogen atmosphere with heating rate of 5 °C/min.

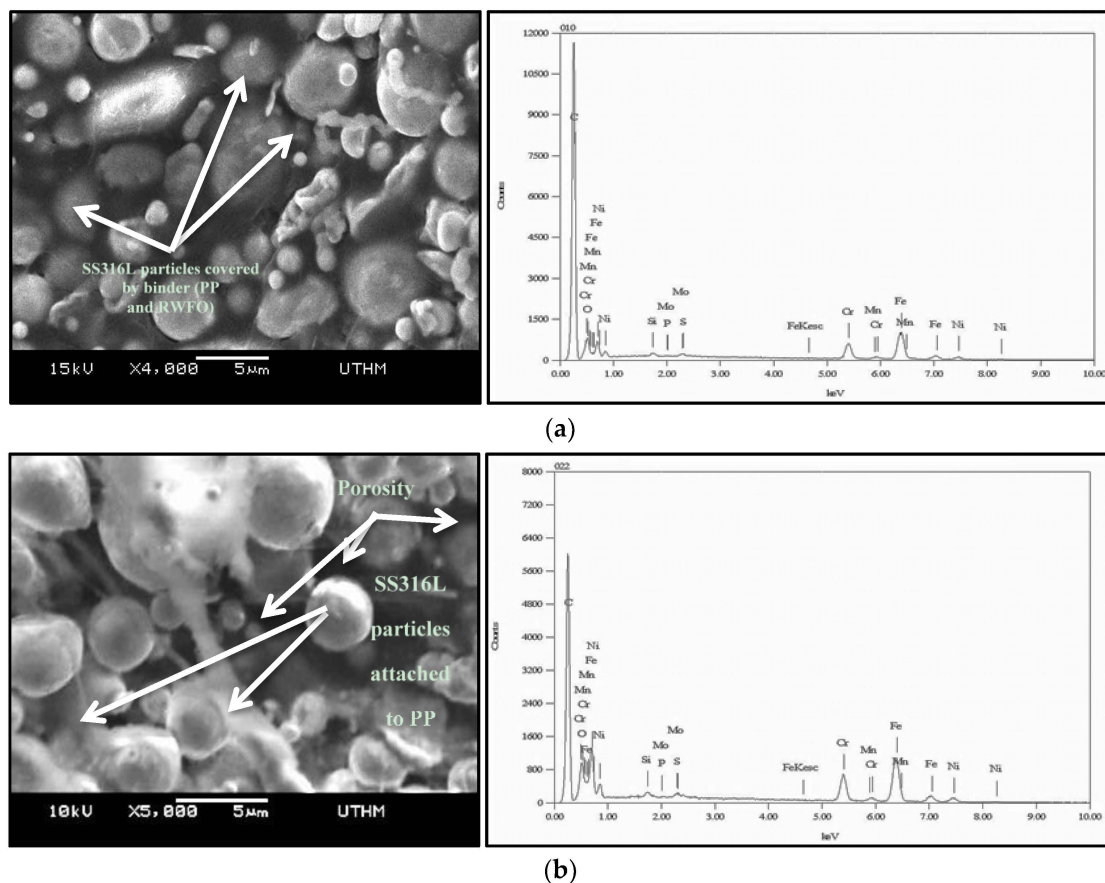


**Figure 15.** Scanning Electron Microscope (SEM) and Energy Dispersive Spectroscopy (a) Green compact morphology (b) green compact after 3 h solvent extraction.

#### 4. Conclusions

Rheological behavior of 316L stainless steel feedstock with RWFO as binder components has been analyzed. It is found that pseudoplastic behavior occurs for all binder formulations with viscosity decrease with increasing shear rate. The viscosity decreases with the increasing quantity of RWFO in the binder system showing that lubrication is much influenced by the quantity of RWFO. However the flow activation energy and moldability index shows that binder formulation of F2 is better which strongly indicates that the optimal feedstock formulation between PP and RWFO is a 20/20 volumetric ratio. This might be due to the contents of the stearic and oleic acids components inside the RWFO being less able to strongly influence the wettability of the feedstock [24]. It is also indicative that the RWFO can be used as a sustainable binder system in MIM and further improvement of the binder ratio can be done by additional stearic acids in the binder systems.

F2 feedstock formulation will then be injected to form green compact as shown in Figure 15a and solvent debound was done using heptane and hexane as the organic solvent with temperatures of 40 °C, 50 °C, and 60 °C. From the results above hexane is chosen to be the suitable organic solvent with temperature of 60 °C. This is due to hexane showing a high diffusion rate and percent weight loss of RWFO during extraction process. The results also show no crack formation on the surface of the green compact and quickest extraction can be accomplished within 3 to 4 h.

**Acknowledgments:** Authors are grateful for the support of this work by the Office of Advanced Manufacturing and Materials Center of Universiti Tun Hussein Onn Malaysia for helpful in preparing samples and analysis.

**Author Contributions:** Mohd Halim Irwan Ibrahim and Azriszul Mohd Amin performed the experimental work. Mohd Halim Irwan Ibrahim and Azriszul Mohd Amin wrote the paper. Mohd Halim Irwan Ibrahim,

Azriszul Mohd Amin, Rosli Asmawi and Najwa Mustafa contributed to the analyses, interpretation and discussion of results.

**Conflicts of Interest:** The authors declare no conflict of interest.

## References

1. German, R.M.; Bose, A. *Injection Molding of Metals and Ceramics*; Metal Powder Industries Federation: Princeton, NJ, USA, 1997.
2. Abolhasani, H.; Muhamad, N. A new starch-based binder for metal injection molding. *J. Mater. Process. Technol.* **2010**, *210*, 961–968. [[CrossRef](#)]
3. Afian, M.; Subuki, I.; Abdullah, N. The influence of palm stearin content on the rheological behavior of 316L stainless steel mim compact. *J. Sci. Technol.* **2012**, *2*, 1–14.
4. Ahn, S.; Jin, S.; Lee, S.; Atre, S.V.; German, R.M. Effect of powders and binders on material properties and molding parameters in iron and stainless steel powder injection molding process. *Powder Technol.* **2009**, *193*, 162–169. [[CrossRef](#)]
5. Ibrahim, M.H.I.; Muhamad, N.; Sulong, A.B.; Jamaludin, K.R. Optimization of Micro Metal Injection Molding with Multiple Performance Characteristics using Grey Relational Grade. *Chiang Mai J. Sci.* **2011**, *38*, 231–241.
6. Karatas, C.; Kocer, A.; Ünal, H.I.I.; Saritas, S. Rheological properties of feedstocks prepared with steatite powder and polyethylene-based thermoplastic binders. *J. Mater. Process. Technol.* **2004**, *152*, 77–83. [[CrossRef](#)]
7. Huang, B.; Liang, S.; Qu, X. The rheology of metal injection molding. *J. Mater. Process. Technol.* **2003**, *137*, 132–137. [[CrossRef](#)]
8. Brandtland, G.H. United Nation Report of the World Commission on Environment and Development: Our Common Future. Available online: <http://www.un-documents.net/wced-ocf.htm> (accessed on 21 December 2015).
9. Gulsoy, H.O.; German, R.M. Production of micro-porous austenitic stainless steel by powder injection molding. *Mater. Sci.* **2008**, *58*, 295–298. [[CrossRef](#)]
10. Kwon, T.H.; Ahn, S.Y. Slip characterization of powder/binder mixtures and its significance in the filling process analysis of powder injection molding. *Powder Technol.* **1995**, *85*, 45–55. [[CrossRef](#)]
11. Khakbiz, M.; Simchi, A.; Bagheri, R. Investigation of rheological behavior of 316L stainless steel—3 wt. % TiC powder injection molding feedstock. *Powder Metall.* **2005**, *48*, 144–150. [[CrossRef](#)]
12. Supriadi, S.; Baek, E.R.; Choi, C.J.; Lee, B.T. Binder system for STS 316 nanopowder feedstocks in micro-metal injection molding. *J. Mater. Process. Technol.* **2007**, *188*, 270–273. [[CrossRef](#)]
13. Omar, M.A.; Subuki, I.; Abdullah, N.S.; Zainon, N.M.; Roslani, N. Processing of Water-Atomised 316L Stainless Steel Powder Using Metal-Injection Processes. *J. Eng. Sci.* **2012**, *8*, 1–13.
14. Salmah, H.; Lim, B.Y.; Teh, P.L. Rheological and thermal properties of palm kernel shell-filled low-density polyethylene composites with acrylic acid. *J. Thermoplast. Compos. Mater.* **2012**. [[CrossRef](#)]
15. Mustafa, N.; Ibrahim, M.H.I.; Asmawi, R.; Amin, A.M.; Masrol, S.R. Green Strength Optimization in Metal Injection Molding Applicable with a Taguchi Method. *Appl. Mech. Mater.* **2015**, *773–774*, 115–117. [[CrossRef](#)]
16. Canakci, M. The potential of restaurant waste lipids as biodiesel feedstocks. *Bioresour. Technol.* **2007**, *98*, 183–190. [[CrossRef](#)] [[PubMed](#)]
17. Zaky, M.T. Effect of solvent debinding variables on the shape maintenance of green molded bodies. *J. Mater. Sci.* **2004**, *39*, 3397–3402. [[CrossRef](#)]
18. Zaky, M.T.T.; Soliman, F.S.S.; Farag, A.S.S. Influence of paraffin wax characteristics on the formulation of wax-based binders and their debinding from green molded parts using two comparative techniques. *J. Mater. Process. Technol.* **2009**, *209*, 5981–5989. [[CrossRef](#)]
19. Yang, W.; Yang, K.; Wang, M.; Hon, M. Solvent debinding mechanism for alumina injection molded compacts with water-soluble binders. *Ceram. Int.* **2003**, *29*, 745–756. [[CrossRef](#)]
20. Ragauskas, A.M.E.; Pu, Y.; Ragauskas, A.J. Biodiesel from grease interceptor to gas tank. *Energy Sci. Eng.* **2013**, *1*, 42–52. [[CrossRef](#)]
21. Williams, J.B.; Clarkson, C.; Mant, C.; Drinkwater, A.; May, E. Fat, oil and grease deposits in sewers: Characterisation of deposits and formation mechanisms. *Water Res.* **2012**, *46*, 6319–6328. [[CrossRef](#)] [[PubMed](#)]

22. Bart, J.C.J.; Gucciardi, E.; Cavallaro, S. Renewable feedstocks for lubricant production. In *Biolubricants Science and Technology*; Woodhead Publishing Ltd.: Abington, UK, 2013; pp. 1–128.
23. Keener, K.M.; Ducoste, J.J.; Holt, L.M. Properties Influencing Fat, Oil, and Grease Deposit Formation. *Water Environ. Res.* **2008**, *80*, 2241–2246. [[CrossRef](#)] [[PubMed](#)]
24. He, X.; Francis, L.; Leming, M.L.; Dean, L.O.; Lappi, S.E.; Ducoste, J.J. Mechanisms of Fat, Oil and Grease (FOG) deposit formation in sewer lines. *Water Res.* **2013**, *47*, 4451–4459. [[CrossRef](#)] [[PubMed](#)]
25. Popkin, B.M. Urbanization, Lifestyle Changes and the Nutrition Transition. *World Dev.* **1999**, *27*, 1905–1916. [[CrossRef](#)]
26. Baines, T.; Brown, S.; Benedettini, O.; Ball, P. Examining green production and its role within the competitive strategy of manufacturers. *J. Ind. Eng. Manag.* **2013**, *5*, 53–87. [[CrossRef](#)]
27. Chan, H. Removal and recycling of pollutants from Hong Kong restaurant wastewaters. *Bioresour. Technol.* **2010**, *101*, 6859–6867. [[CrossRef](#)] [[PubMed](#)]
28. Amin, A.M.; Ibrahim, M.H.I.; Asmawi, R.; Mustafa, N. The Influence of Sewage fat Composition on Rheological Behavior of Metal Injection Molding. *Appl. Mech. Mater.* **2014**, *660*, 38–42. [[CrossRef](#)]
29. Sotomayor, M.E.E.; Várez, A.; Levenfeld, B. Influence of powder particle size distribution on rheological properties of 316L powder injection molding feedstocks. *Powder Technol.* **2010**, *200*, 30–36. [[CrossRef](#)]
30. Ibrahim, M.H. *Optimization of MicroMetal Injection Molding Parameter by Design of Experiment Method*; Universiti Kebangsaan Malaysia: Selangor, Malaysia, 2011.
31. Sotomayor, M.E.; Levenfeld, B.; Várez, A. Powder injection molding of premixed ferritic and austenitic stainless steel powders. *Mater. Sci. Eng. A* **2011**, *528*, 3480–3488. [[CrossRef](#)]
32. Jaggi, H.S.; Kumar, Y.; Satapathy, B.K.; Ray, A.R.; Patnaik, A. Analytical interpretations of structural and mechanical response of high density polyethylene/hydroxyapatite bio-composites. *Mater. Des.* **2012**, *36*, 757–766. [[CrossRef](#)]
33. Ghazavi, M.A.; Fallahipanah, M.; Jeshvaghani, H.S. A feasibility study on beef tallow conversion to some esters for biodiesel production. *Int. J. Recycl. Org. Waste Agric.* **2013**, *2*, 1–4. [[CrossRef](#)]
34. Adames, J.M. Characterization of Polymeric Binders for Metal Injection Molding (MIM) Process. Ph.D. Thesis, The University of Akron, Akron, OH, USA, December 2007.
35. Li, L.; Liu, X.Q.; Luo, F.H.; Yue, J.L. Effects of surfactant on properties of MIM feedstock. *Trans. Nonferrous Met. Soc. China* **2007**, *17*, 1–8. [[CrossRef](#)]
36. Ibrahim, M.H.I.; Muhamad, N.; Sulong, A.B. Rheological Investigation of Water Atomised Stainless Steel Powder for Micro Metal Injection Molding. *Int. J. Mech. Mater. Eng.* **2009**, *4*, 1–8.
37. Aggarwal, G.; Park, S.J.; Smid, I. Development of niobium powder injection molding: Part I. Feedstock and injection molding. *Int. J. Refract. Met. Hard Mater.* **2006**, *24*, 253–262. [[CrossRef](#)]
38. Hidalgo, J.; Jiménez-Morales, A.; Torralba, J.M. Torque rheology of zircon feedstocks for powder injection molding. *J. Eur. Ceram. Soc.* **2012**, *32*, 4063–4072. [[CrossRef](#)]
39. Liu, H.; Mou, J.; Cheng, Y. Impact of pore structure on gas adsorption and diffusion dynamics for long-flame coal. *Nat. Gas Sci. Eng.* **2015**, *22*, 203–213. [[CrossRef](#)]

